*Physicochem. Probl. Miner. Process., 60(1), 2024, 185334*

http://www.journalssystem.com/ppmp

Physicochemical Problems of Mineral Processing

ISSN 1643-1049


# Comparative investigation on capture characteristics of chalcopyrite and hematite in PHGMS process

**Mingyu Tao, Luzheng Chen, Pulin Dai, Zixing Xue, Hang Chen**

Faculty of Land and Resources Engineering, Kunming University of Science and Technology, Kunming 650093, Yunnan, China

Corresponding author. xue_zixing@126.com (Zixing Xue)

**Abstract:** Pulsating high-gradient magnetic separation (PHGMS) is a promising method of separating chalcopyrite from other minerals with similar floatability. However, the capture characteristics of chalcopyrite in the PHGMS process remain poorly understood. In this study, the difference in the capture capacity of chalcopyrite and hematite, a typical weak magnetic mineral, was theoretically compared. The effects of the key operating parameters, i.e., magnetic induction, slurry flow rate, and magnetic wire diameter, on the capture difference between chalcopyrite and hematite, were investigated through experimental verification. The comparison results showed that chalcopyrite shared a similar capture trend with hematite. The capture mass weight of the matrix decreased with an increase in the pulsating frequency, slurry flow rate, and magnetic wire diameter, but it increased with improved magnetic induction. However, chalcopyrite exhibited a smaller capture mass weight due to its lower susceptibility, which required a higher magnetic induction (1.4 T), slower flow rate (1.5 cm/s), lower pulsating frequency (150 rpm), and smaller matrix diameter (1 mm) for higher efficient recovery of chalcopyrite. As the magnetic induction increased from 0.8 T to 1.6 T, the chalcopyrite recovery improved from 65.84% to 75.80%. These findings provide valuable information for improving the utilization of chalcopyrite.

***Keywords:*** pulsating high-gradient magnetic separation, static buildup model, chalcopyrite, hematite, matrix capture

## 1. Introduction

Chalcopyrite ($CuFeS_2$) is the most abundant mineral in copper ore, and more than 70% of the world's copper is extracted from chalcopyrite (Mahajan et al., 2007; Zhao et al., 2019). For economic utilization of chalcopyrite, an enrichment process from lower grades before metallurgical processes is necessary. Flotation is currently considered the most efficient method for concentrating chalcopyrite (Qiu et al., 2022a; Luo et al., 2022). However, separating chalcopyrite from other sulfide minerals using flotation has some obvious drawbacks due to the large consumption of reagents: the process can be very complicated due to their similar floatability (Yan et al., 2020; Liu and Zhang., 2024), and the reagent used can increase the production cost and bring pollution risks. In comparison, pulsating high-gradient magnetic separation (PHGMS) has emerged as a promising alternative method due to its cost and environmental-friendly advantages (Zykin et al., 2022; Qiu et al., 2022b; Zheng et al., 2023). For example, recent reports have proved that pulsating high-gradient magnetic separation (PHGMS) is effective for the separation of chalcopyrite from other minerals with similar floatability, such as molybdenite and talc (Chen et al., 2021; Xian et al., 2022). However, the capture mechanism of matrix onto chalcopyrite remains unclear. Therefore, a comparative investigation on the capture characteristics of chalcopyrite and hematite, a typical weakly magnetic mineral that has been maturely extracted by PHGMS, would help to have a deeper understanding of the treatment and separation process of chalcopyrite.

Static buildup model (SBM) is an analytical approach to predict the upstream buildup profile of a circular matrix in high-gradient magnetic separation (HGMS), it is often used to predict the capturing capacity of a magnetic matrix for certain types of particles (Xue et al., 2022). In this study, the

DOI: 10.37190/ppmp/185334

accumulation profile of chalcopyrite was theoretically analyzed using a static buildup model (SBM) and compared with hematite. Then, a comparative experimental study on chalcopyrite and hematite was carried out in an SLon-100 separator. The effects of magnetic induction, slurry flow rate, pulsating frequency, and magnetic matrix diameter on the capture mass weight of these two minerals were analyzed in depth. The results from this investigation have provided vital information for the eco-friendly and cost-effective separation of chalcopyrite from sulfide minerals using the PHGMS method.

## 2. Materials and methods

### 2.1. Materials

The selected mineral samples of high-purity chalcopyrite and hematite were produced in Yunnan Province, China. Large pieces of mineral ore are crushed with a hammer and sieved to a size range below 2 mm. Every 100 g sample was then ground in a porcelain ball mill for about 5 min. After all the samples were prepared, they were mixed and ready for analysis and tests. X-ray diffraction (XRD) results as shown in Fig. 1 indicated that the samples used were in high purity. The size distributions of the chalcopyrite and hematite were measured by sieving and screening results listed in Table 1 demonstrating similar particle size characteristics that fine minerals account for the main part. The volume susceptibility values of the chalcopyrite and hematite samples, which were determined using a high-intensity magnetometer, were 0.0005 and 0.003, respectively.

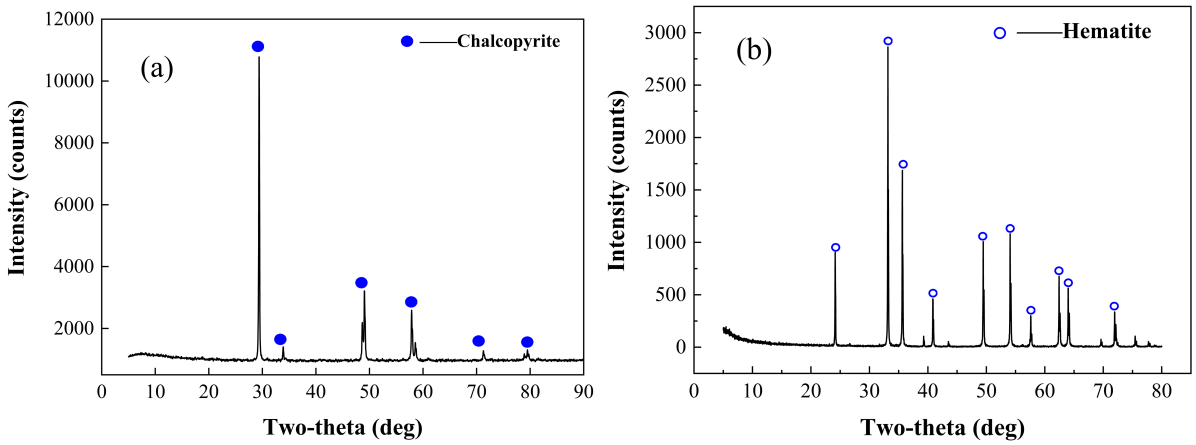


Fig. 1. XRD pattern of chalcopyrite and hematite

Table 1. Screening results of the samples

| Particle Size (mm) | Weight of Chalcopyrite (%) | Weight of Hematite (%) |
|---|---|---|
| +0.074 | 25.83 | 26.83 |
| −0.074+0.045 | 17.91 | 20.71 |
| −0.045+0.038 | 5.54 | 4.19 |
| −0.038 | 50.72 | 48.27 |
| +0.074 | 25.83 | 26.83 |

### 2.2. Methods

#### 2.2.1. Equipment

A cyclic SLon-100 PHGMS separator, manufactured by SLon Magnetic Separator Co., Ltd., in Jiangxi Province, China, was used for the capturing tests. As shown in Fig. 2, the separator is mainly composed of magnetic poles, magnetic yoke, excitation coils, and pulsating mechanisms. The separation chamber of the separator was first filled with water to fully immerse the rod matrix in the water, and the pulsating power of water generated by the pulsating structure was transferred to the separation chamber.

Simultaneously, the excitation current was switched on to provide a uniform magnetic field to the separation chamber. Then, the slurry was fed into the feed box, and magnetic particles were captured on the surface of the matrix due to the magnetic and fluid forces. Meanwhile, nonmagnetic particles passed through the matrix as nonmagnetic products. When a batch of feed was completed, the excitation current was cut off, and the magnetic product was obtained after washing.

The captured particles onto the elements were washed out with clean water, dried, and weighed as concentrates. The mass weight of magnetic particles captured onto each element was used to evaluate the capture performance (Zeng et al., 2019). In this study, each batch of 50 g samples was fed after 10 min stirring in the slurry, and each experiment was repeated three times to get an averaged final result.

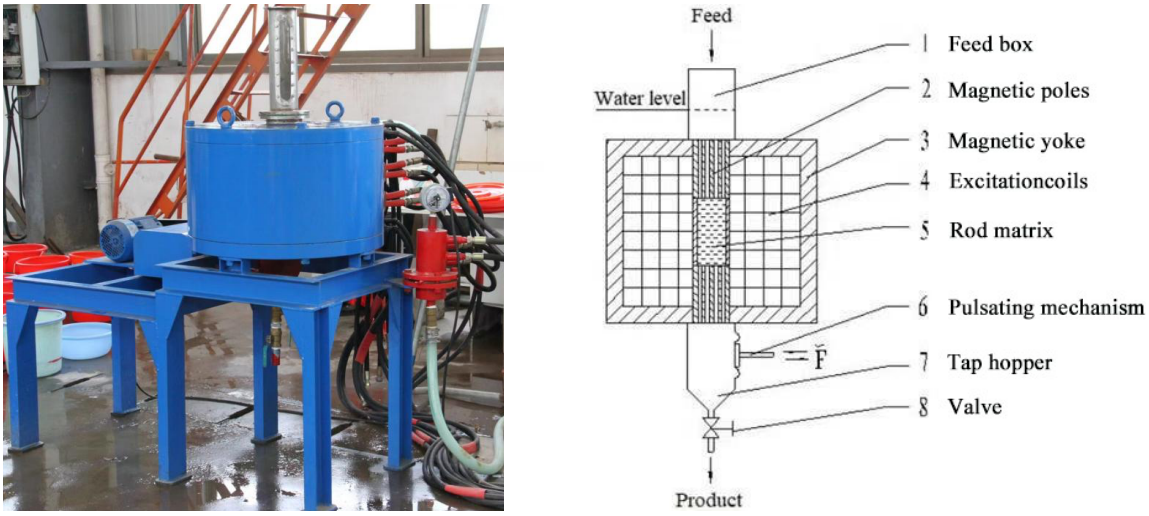


Fig. 2. SLon-100 cyclic PHGMS separator

### 2.2.2. Description of SBM theory

The static buildup model (SBM) is a steady-state theory based on force analysis of each layer of accumulation (Xue et al., 2022). The SBM hypothesis states that particles already contact the surface of a deposit without having to pay attention to the particle trajectories before their arrival. The role of SBM is to determine the accumulation range using force-equilibrium analysis. In longitudinal HGMS, the flow is parallel to the applied magnetic field, and besides flow and magnetic field are both perpendicular to the matrix axis. Fig. 3 shows the components of the forces that act on the particle at rest on the matrix surface.

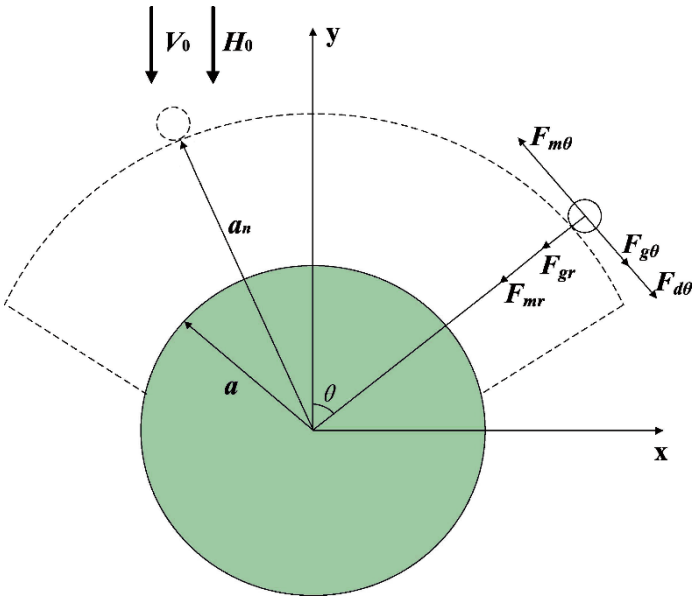


Fig. 3. Components of the forces acting on the particle that is in contact with the matrix

For a spherical particle at rest on the matrix, the radial and tangential components of the magnetic force are expressed in Eqs. (1) and (2), respectively (Mulliken., 1955).

$$F_{mr} = -\frac{8}{3}\pi b^3 \mu_0 \kappa \frac{B_1}{r^3}\left(H_0 \cos 2\theta + \frac{B_1}{r^2}\right) \quad (1)$$

$$F_{m\theta} = -\frac{8}{3}\pi b^3 \mu_0 \kappa \frac{B_1}{r^3} H_0 \sin 2\theta \quad (2)$$

where $b$ and $\kappa$ are the radius and volume susceptibility of the particle, respectively, $\mu_0$ is the vacuum permeability, which equals $4\pi \times 10^{-7}$ H/m, $r$ is the distance between the particle center and matrix, $H_0$ is the applied magnetic field strength (Zheng et al., 2017), and $a$ is the radius of the matrix. $B_1$ is a coefficient determined by the magnetization state of the matrix, as expressed in Eq. (3).

$$B_1 = H_0 a^2 \quad (3)$$

The gravity forces in the radial and tangential directions are expressed in Eqs. (4) and (5), respectively.

$$F_{gr} = -\frac{4}{3}\pi b^3 \left(\rho_p - \rho_f\right) g \cos\theta \quad (4)$$

$$F_{g\theta} = \frac{4}{3}\pi b^3 \left(\rho_p - \rho_f\right) g \sin\theta \quad (5)$$

where $\rho_p$ and $\rho_f$ are the density of the particle and fluid respectively. The particles are only dragged in the tangential direction. Thus, the Blasius solution (Oliveira et al., 2012) for the shear stress is introduced to fix this problem using Eq. (6).

$$F_{d\theta} = -\frac{\pi^2 b^2}{4}\rho_f V_0^{3/2}\left(\frac{\nu}{r}\right)^{1/2}\left(6.973\theta - 2.732\theta^3 + 0.292\theta^5 - 0.0183\theta^7 + 0.000043\theta^9 - 0.000115\theta^{11}\right) \quad (6)$$

where $V_0$ is the initial velocity of the fluid, v is the kinematic viscosity of the fluid. Integrating Eqs. (1), (2), (4), (5), and (6) allows calculation of the net forces in the radial and tangential directions, as expressed in Eqs. (7) and (8), respectively.

$$F_{netr} = F_{mr} + F_{gr} \quad (7)$$

$$F_{net\theta} = F_{m\theta} + F_{g\theta} + F_{d\theta} \quad (8)$$

The θ value that satisfies $F_{netr} = 0$ and $F_{net\theta} = 0$ is calculated, and the smaller of the two angles, i.e., $\theta_c$, is selected to determine the accumulation range of each layer (Zheng et al., 2015). This decision is made from layer to layer from the inside to outside. As the accumulation continues, $r$ expands, and for the $n^{th}$ layer of the particles.

$$r = a + b + (n-1)\sqrt{3} \quad (9)$$

To avoid singularity at the front stagnation point, the accumulation is assumed to stop when $\theta_c < 10°$, which defines the final layer and the saturated accumulation profile.

### 2.2.3. Comparison of predicted accumulation profiles of chalcopyrite and hematite

In the SBM analysis, the volume susceptibility of chalcopyrite and hematite were specified as 0.003 and 0.0005, respectively. The particles were assumed as spherical with a diameter of 0.074 mm, and feeding velocity V0 was set as 0.2 m/s. The effect of magnetic induction B0 on the predicted accumulation profile of the two minerals was investigated under 0.8, 1.2, and 1.6 T in Fig. 4.

As shown in Fig. 4, the predicted accumulation profile of chalcopyrite and hematite both expand with the increment of magnetic induction and chalcopyrite occupies less area than hematite when they are exposed to the same magnetic induction. For example, when B0 equals 0.8 T, the predicted accumulation area of hematite is over 5 times larger than chalcopyrite. However, by increasing the magnetic induction to 1.6 T, the capturing performance of chalcopyrite can improve to an encouraging level even larger than that of hematite at 0.6 T.

The SBM analysis indicated that chalcopyrite was able to be effectively captured by a matrix as long as operation conditions permit. So, in the next part, experiments were conducted to investigate the capture characteristics of chalcopyrite by comparing its capturing behavior with hematite.

## 3. Results and discussion

### 3.1. Effect of magnetic induction

In the PHGMS process, magnetic induction has a decisive effect on the capture characteristics, so it

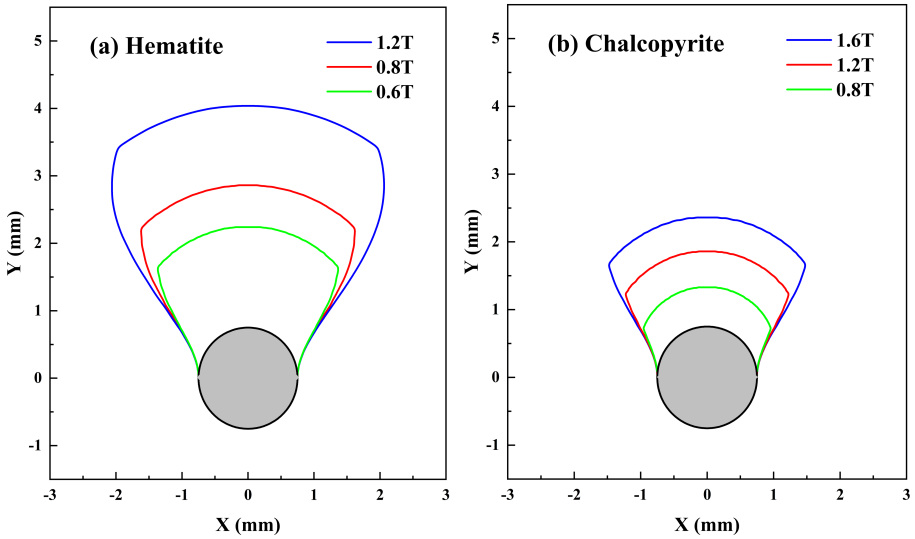


Fig. 4. Evolution of the saturated accumulation profile of upstream deposit along with magnetic induction: (a) hematite and (b) chalcopyrite

was investigated. The following parameters were used in this experiment: a pulsation frequency of 200 rpm, a slurry flow rate of 3 cm/s, a magnetic-medium wire diameter of 1.5 mm, and magnetic inductions of 0.8, 1.0, 1.2, 1.4, and 1.6 T. Figure 5 shows that the chalcopyrite and hematite exhibited different capture characteristics. When the magnetic induction increased from 0.8 to 1.6 T, the recovery of chalcopyrite increased from 65.84% to 75.80% while the hematite recovery stayed unchanged at a high level above 96%. It is worthwhile mentioning that recovery equals to yield of the magnetic concentrate in a single mineral test.

Under the same magnetic-induction intensity, the recovery of chalcopyrite was lower than that of hematite, because the magnetic force of chalcopyrite was weaker due to smaller susceptibility (chalcopyrite and hematite were 0.0005 and 0.003, respectively), resulting in fewer chalcopyrite particles captured by the magnetic matrix (Liu, 1994). Therefore, a relatively high field intensity (above 1.4 T) is required to achieve effective recovery of chalcopyrite. Fortunately, with the development of manufacturing technology, existing large-scale high-gradient magnetic separators are now capable of providing a background magnetic field up to 1.8 T. This opens the possibility for industrial application of high-gradient magnetic separation for chalcopyrite-bearing ore. In a previous raw sample test done by Chen et al. (2021), the magnetic product from the pulsating HGMS process assays 22–24% Cu at 60–70% Cu recovery. This shows that it is possible to separate chalcopyrite by magnetic separation in industrial applications.

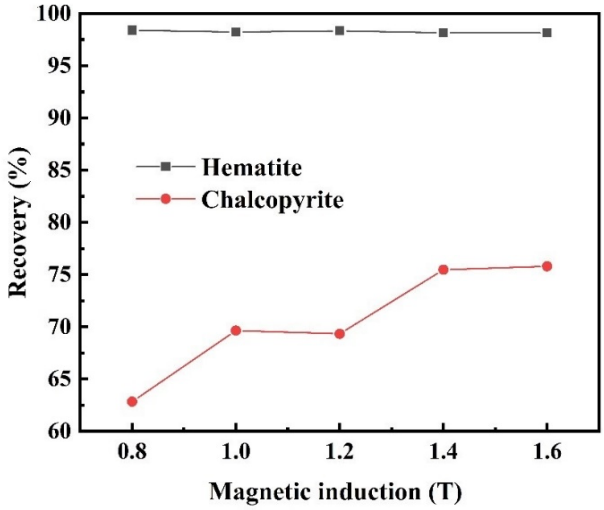


Fig. 5. Effect of magnetic induction on the capture weight of the two pure minerals

### 3.2. Effect of slurry flow rate

Slurry flow rate is a key factor in the PHGMS industry, a too fast or too slow flow rate affects the production capacity of the matrix (Chen et al., 2010). In this part, the slurry flow rate at 1.5, 2, 3, 5, and 7 cm/s were tested by fixing the following parameters at a pulsation frequency of 200 rpm, a magnetic induction of 1.4 T, a magnetic-medium wire diameter of 1.5 mm.

As shown in Fig. 6, the recovery of the two minerals both decreased with increasing slurry flow rate. When the slurry flow rate increases from 1.5 cm/s to 7 cm/s, the chalcopyrite recovery decreases from 80.68% to 59.62%. However, the recovery of hematite ore remains higher than 93%.

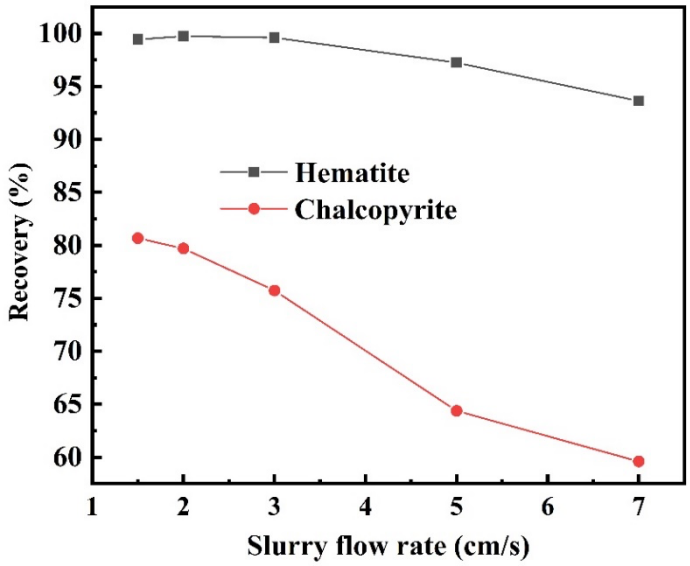


Fig. 6. Effect of slurry flow rate on the capture weight of the two pure minerals

Under the same slurry flow rate, the recovery of chalcopyrite was always lower than that of hematite. With the increase in slurry flow rate, the recovery of chalcopyrite drops more rapidly than that of hematite. This could be attributed to the weaker magnetic force subjected by chalcopyrite, making it less capable of resisting the intensive drag force caused by increasing flow rate. Moreover, a higher flow rate means less retention time of particles in the separation chamber, which is more detrimental to the capture of chalcopyrite particles due to weaker magnetic force. The results also demonstrated that a highly efficient recovery of chalcopyrite required a relatively low feeding velocity, so in future industrial production, low throughput is predictable.

### 3.3. Effect of pulsating frequency

Pulsating frequency can significantly improve the looseness degree and greatly affect the drag force subjected to particles. In this experiment, the effect of pulsating frequency was investigated, with other parameters fixed at a magnetic induction of 1.4 T, a slurry flow rate of 3 cm/s, and a magnetic-medium wire diameter of 1.5 mm. As shown in Fig. 7, the recovery of chalcopyrite significantly decreased from 75.52% to 32.08% when the pulsating frequency increased from 150 to 300 rpm. Meanwhile, the recovery of hematite remained unchanged. This phenomenon could also be explained by the weaker magnetic force subjected by chalcopyrite, making it less capable of resisting the intensive drag force brought by increasing pulsation frequency (Chen et al., 2017). The results indicated that intensive pulsating frequency is adverse to the highly efficient recovery of chalcopyrite, so in future industrial production, a relatively weak pulsating strength is recommended.

### 3. 4. Effect of matrix diameter

The diameter of the matrix is another factor that determines the magnetic field gradient. The smaller the diameter, the larger will be the magnetic field gradient (Chen et al., 2014; Chen et al., 2017). The

following parameters are chosen in this experiment: a pulsating frequency of 200 rpm, a magnetic induction of 1.4 T, and a slurry flow rate of 3 cm/s. The experimental results shown in Fig. 8 indicated that when the matrix diameter increased from 1.0 to 2.0 mm, the recovery of chalcopyrite slowly decreased while that of hematite remained unchanged. This phenomenon can be explained by other parameters being unchanged, the magnetic force decreases as the diameter of the matrix increases (Chen et al., 2014; Chen et al., 2017). The results implied that a matrix with a smaller size was conductive to the capture of chalcopyrite, future industrial production should consider this.

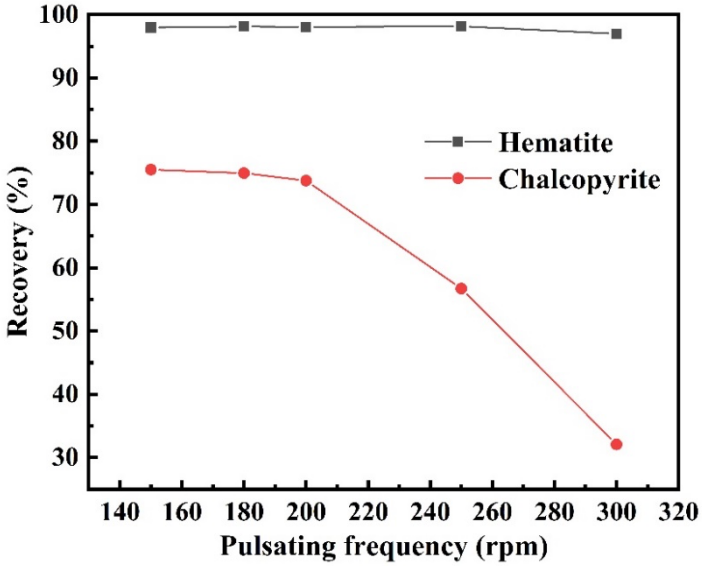


Fig. 7. Effect of magnetic pulsating frequency on the capture weight of the two pure minerals

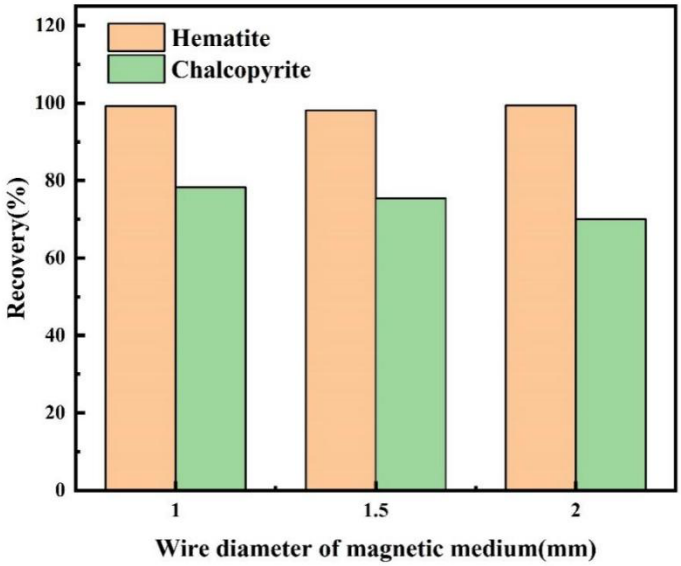


Fig. 8. Effect of magnetic-medium wire diameter on the capture weight of the two pure minerals

## 4. Conclusions

Pulsating high-gradient magnetic separation (PHGMS) is a promising method for separating chalcopyrite, but the capture mechanism of a matrix for chalcopyrite remains unclear in mineral processing. In this study, the SBM model was used to predict the capture capacity of chalcopyrite in comparison with that of hematite. The results indicated that the accumulation area of chalcopyrite was much smaller than that of hematite, but it could be enlarged by enhancing magnetic induction. Experiments conducted in the SLon-100 cyclic PHGMS separator confirmed the predicted results by the SBM model, and more experiments further indicated that a high-efficient separation of chalcopyrite

requires a relatively strong magnetic induction (1.4 T), low feed velocity (1.5 cm/s), gentle pulsation strength (150 rpm) and small matrix diameter (1 mm). As the magnetic induction increased from 0.8T to 1.6T, the chalcopyrite recovery improved from 65.84% to 75.80%. It indicates that higher magnetic induction enhances the efficiency of the recovery process for chalcopyrite. However, the slurry flow rate, pulsating frequency, and matrix diameter have a negative correlation to the recovery of chalcopyrite. These findings provide valuable information for improving the utilization of chalcopyrite.

**Acknowledgments**

This work was supported from the National Natural Foundations of China (52104255), the High-Level Talent Recruitment Program of Yunnan Province (No. 140520210124), and the Basic Research Program of Yunnan Province (202201AU070139).

**Reference**

CHEN, L., XIONG, D., and HUANG, H., 2010. *Pulsating high-gradient magnetic separation of fine hematite from tailings*. Miner. Metall. Process. 26(3), 163-168.

CHEN, L., DING, L., ZHANG, H., and HUANG, J., 2014. *Slice matrix analysis for combinatorial optimization of rod matrix in PHGMS*. Miner. Eng. 58 (1), 104-107.

CHEN, L., LIU, W., ZENG, J., and REN, P., 2017. *Quantitative investigation on magnetic capture of single wires in pulsating HGMS*. Powder Technol. 313, 54-59.

CHEN, L., XIONG, T., XIONG, D., YANG, R., PENG, Y., SHAO, Y., XU, J., and ZENG, J., 2021. *Pulsating HGMS for industrial separation of chalcopyrite from fine copper-molybdenun co-flotation concentrate*. Miner. Eng. 170, 106967.

LUO, Q., SHI, Q., LIU, D., LI, B., and JIN, S., 2022. *Effect of deep oxidation of chalcopyrite on surface properties and flotation performance*. Int. J. Min. Sci. Technol. 32(4), 907-914.

LIU, X., and ZHANG, X., 2024. *Welan gum as a new depressant for the flotation separation of chalcopyrite from talc*. Chem. Phys. 578, 112139.

LIU, S., 1994. *Magnetoelectric beneficiation*. Central South University of Technology Press. 337 (in Chinese).

MAHAJAN, V., MISRA, M., and ZHONG, K., 2007. *Enhanced leaching of copper from chalcopyrite in hydrogen peroxide-glycol system*. Miner. Eng. 20(7), 670-674.

MULLIKEN, R. S. 1955. *Electronic population analysis on LCAO–MO molecular wave functions*. I. Chem. Phys. 23(10), 1833.

OLIVEIRA, C., LIMA, G. F., ABREU, H. A and DUARTE, H. A., 2012. *Reconstruction of the chalcopyrite surfaces – a DFT study*. Chem. Phys. 116(10), 6357-6366.

QIU, X., YANG, H., CHEN, G., TONG, L., JIN, Z., and ZHANG, Q., 2022a. *Interface behavior of chalcopyrite during flotation from cyanide tailings*. Int. J. Miner., Metall. Mater. 29(3), 439-445.

QIU, T., YANG, L., YAN, H., ZHANG, H., CUI, L., and LIU, X., 2022b. *The mechanism of the effect of pre-magnetized butyl xanthate on chalcopyrite flotation*. Minerals. 12(2), 209.

XIAN, Y., HONG, Y., LI, Y., LI, X., ZHANG, S., and CHEN, L., 2022. *Pulsating high-gradient magnetic separation of chalcopyrite and talc*. Miner. Eng. 178, 107410.

XUE, Z., WANG, Y., ZHENG, X., LU, D., SUN, Z., and HU, Z., 2022. *Simulation of particle accumulation in high gradient magnetic separation based on static buildup model (SBM)*. Miner. Eng. 175, 107290.

YAN, X., FEI, Y., ZHONG, L., and WEI, W., 2020. *Arsenic stabilization performance of a novel starch-modified Fe-Mn binary oxide colloid*. The Science of the Total Environment. 707, 136064.

ZENG, J., TONG, X., REN, P., and CHEN, L., 2019. *Theoretical description on size matching for magnetic element to independent particle in high gradient magnetic separation*. Miner. Eng. 135, 74-82.

ZHAO, H., ZHANG, Y., ZHANG, X., QIAN, L., SUN, M., YANG, Y., ZHANG, Y., WANG, J., KIM, H., and QIU, G., 2019. *The dissolution and passivation mechanism of chalcopyrite in bioleaching: An overview*. Miner. Eng. 136, 140-154.

ZHENG, X., WANG, Y., and LU, D., 2015. *A realistic description of influence of the magnetic field strength on high gradient magnetic separation*. Miner. Eng. 79(1), 94-101.

ZHENG, X., WANG, Y., LU, D., and LI, X. 2017. *Theoretical and experimental study on elliptic matrices in the transversal high gradient magnetic separation*. Miner. Eng. 111(1), 68-78.

ZHENG, Y., HUANG, Y., HU, P., QIU, X., LV, J., and BAO, L., 2023. *Flotation behaviors of chalcopyrite and galena using ferrate（VI） as a depressant*. Int. J. Min. Sci. Technol. 33(1), 93-103.

ZYKIN, M.A., BUSHEVA, E.V., AMINOV, T.G., SHABUNINA, G.G., and EFIMOV, N.N., 2022. *Synthesis and magnetic properties of $CuGaSe_2$: Mn manganese-doped chalcopyrites*. Russ. J. Inorg. Chem. 67(2), 150-157.